RI 8016

Bureau of Mines Report of Investigations/1975

Numerical Simulation of Flame-Induced Aerodynamics in a Coal Mine Passageway, Semi-Empirical Model

UNITED STATES DEPARTMENT OF THE INTERIOR

Report of Investigations 8016

Numerical Simulation of Flame-Induced Aerodynamics in a Coal Mine Passageway, Semi-Empirical Model

By Donald N. H. Chi and Henry E. Perlee
Pittsburgh Mining and Safety Research Center, Pittsburgh, Pa.

UNITED STATES DEPARTMENT OF THE INTERIOR
Rogers C. B. Morton, Secretary

Jack W. Carlson, Assistant Secretary–Energy and Minerals

BUREAU OF MINES
Thomas V. Falkie, Director

This publication has been cataloged as follows:

Chi, Donald N H

Numerical simulation of flame-induced aerodynamics in a coal mine passageway, semi-empirical model, by Donald N. H. Chi and Henry E. Perlee. [Washington] U.S. Bureau of Mines [1975]

27 p., illus., tables. (U.S. Bureau of Mines. Report of investigations 8016)

Includes bibliography.

1. Mine fires—Simulation methods. 2. Flame—Simulation methods. I. U.S. Bureau of Mines. II. Perlee, Henry E., jt. auth. III. Title. IV. Title: Aerodynamics in a coal mine passageway. (Series)

TN23.U7 no. 8016 622.06173

U.S. Dept. of the Int. Library

CONTENTS

ILLUSTRATIONS

TABLES

NUMERICAL SIMULATION OF FLAME-INDUCED AERODYNAMICS IN A COAL MINE PASSAGEWAY, SEMI-EMPIRICAL MODEL

by

Donald N. H. Chi[1] and Henry E. Perlee[2]

ABSTRACT

This Bureau of Mines report is concerned with a theoretical study of the aerodynamic response of a single mine entry to flame-induced disturbance. The unsteady, one/dimensional, compressible flow equations were solved using the method of characteristics. This study was primarily undertaken to determine the feasibility of extending the method of characteristics to study the aerodynamic response of complex mine networks. It was demonstrated that although the technique has merit in studying the complex wave interaction in single entries, it appears to be too unwieldly and too expensive for network analysis. Effort was also directed at a further study of the dispersion and filtering characteristic of aerodynamic disturbances in mine passageways.

INTRODUCTION

This is the first of a series of studies directed at obtaining a mathematical description of the history of flame development and propagation in coal mines.

In recent years, coal mine disasters due to fires and explosions have stimulated research in understanding the development of fire disaster because they relate to the interaction between the combustion process and the induced or existing (ventilation) aerodynamic disturbances. Through such understanding, one can develop methods for preventing the propagation of flame in an environment such as a coal mine that contains combustible methane gas and/or coal dust.

It is the current popular opinion that coal mine disasters involving rapidly propagating combustion phenomena are primarily sustained through combustion of the coal dust. It is further maintained that the coal dust combustion process is initiated through the prior ignition and combustion of flammable pockets of methane air. In general, the concentration of coal dust normally suspended in the mine ventilation air is considerably below that required to sustain flame propagation; therefore, it is believed that methane/air

[1]Research physicist.
[2]Supervisory research chemist.

combustion generates aerodynamic disturbances of sufficient magnitude to lift coal dust from the passageway surfaces, primarily the floor, and disperse and suspend it long enough for the flame to reach it and start a coal-dust/air flame. The coal-dust/air combustion subsequently maintains the airflow necessary to provide continued dust lifting and dispersion, and thereby, the process becomes self-supporting.

This research program is concerned primarily with the development of the initial methane/air flames and the associated aerodynamic disturbances.

This investigation is concerned with determining the transient aercdynamic response characteristics of a single mine entry to flame-induced aerodynamic disturbances. Particular emphasis has been placed on determining the feasibility of extending the numerical technique used (the method of characteristics) to conduct similar studies of a complex of mine passageways such as a room-and-pillar in a coal mine. To expedite the study, the authors have neglected any interaction between the flame (or product gases) and the flame-induced disturbances; this topic is treated in a second report (3).[3]

The present study is concerned only with the situation where the methane/air combustion is completed or extinguished and the product gases cooled before any reflected aerodynamic disturbances return to the site of the combustion. For this reason, the interaction of the flame and the returning (reflected) aerodynamic disturbances have not been included.

Most of the investigations (1-2, 5, 8, 10-11, 17) involving coal mine explosions carried out to date in the United States and abroad have been of an experimental nature. It is apparent from the results of these investigations that the propagation characteristics of dust or gas flames are significantly modified by the interaction of the flame with its induced-aerodynamic disturbances; therefore, what is observed in these galleries is not only a function of the combustion chemistry but also, possibly more importantly, a function of the aerodynamic response of the galleries. In other words, geometric factors such as changes in gallery cross-sectional area, gallery length, wall roughness, the presence of junctions and crosscuts, obstructions and others, both ahead and behind the flame front, have pronounced effects on the combustion process. Extreme care is required in applying the results of experimental studies conducted in galleries dissimilar to the actual mine geometry to systems as geometrically complex as coal mines. For example, the optimal location of flame suppressant devices, as determined in a straight smooth-wall gallery, may not be optimal in a complex mine entry possessing entirely different aerodynamic characteristics. On the other hand, if mathematical descriptions can be obtained and proven for flame propagation in a gallery, then this description can be utilized to characterize flame propagation in mine passageway. This is one of the major purposes for conducting these mathematical investigations. In addition, such models could find utility in extending experimental measurements to uninstrumented regions, thereby minimizing the number of recording stations required.

---

[3]Underlined numbers in parentheses refer to items in the list of references preceding the appendix.

Although the fundamental partial differential equations that describe the transient response of compressible fluids are generally too complicated to be solved analytically, the advent of large high-speed digital computers coupled with powerful numerical techniques has quickly brought the field of computational fluid dynamics to its maturity. The validity of these equations has been verified in numerous experiments. The resulting computer code is usually very flexible and can easily be used to conduct parametric studies of the aerodynamic responses of coal mines to isolate the significance of various affects.

ACKNOWLEDGMENT

The authors wish to thank Israel Liebman, Kenneth J. Richmond, and Joseph M. Singer, all of the Pittsburgh Mining and Safety Research Center, Pittsburgh, Pa., for numerous valuable discussions concerning the experimental aspects of this work. We particularly wish to thank Mr. Singer for providing the experimental data cited in this report.

MODEL

It has been observed (1, 11, 13) that the flow fields at a cross section of a flame gallery are fairly uniform except within a distance of a few centimeters from the wall. The implication of this is that a one-dimensional model should adequately describe the aerodynamic characteristics of long-flame galleries of coal mine passageways. To expedite the study, the formation of shocks and the presence of the burned zone have been excluded; these have been taken into account in the second report (3).

Assumptions

The following assumptions have been incorporated in the model:

1. The system is quasi-linear in the sense that the velocity component u in the axial direction x predominates over the two transversal components (v and w) and all field variables are cross-sectional averages.

2. The shearing stresses $\tau_{xy} = \mu \frac{\partial u}{\partial y}$ and $\tau_{xz} = \mu \frac{\partial u}{\partial z}$ are constant denoted as τ_w along the wall.

3. P is a function of x and t only.

4. Body forces are absent.

5. The normal viscous stress $\mu \frac{\partial^2 u}{\partial x^2} \ll \frac{\partial P}{\partial x}$.

6. The process is isentropic.

7. The gas obeys the ideal-gas law.

8. The gas is homogeneous.

9. The gas is always in thermodynamic equilibrium; that is, its thermodynamic state is uniquely determined by any two independent variables.

10. Transport phenomena such as heat conduction and mass diffusion are neglected.

11. The pressure at the open end is ambient (this assumption is acceptable as long as the wavelength of the disturbance is large compared with the gallery diameter).

Governing Equations

A. Ferri and L. G. Mapolitano (6) give the derivation of the continuity or conservation of mass equation in which the flow variables represent averages over the cross-sectional area. Appendix A shows the derivation of the momentum equation including the wall-stress term. The working equations then take on the final form:

$$\frac{\partial \rho}{\partial t} + \frac{\partial \rho u}{\partial x} = 0 \qquad \text{(continuity equation)}, \tag{1}$$

and

$$\frac{\partial u}{\partial t} + u \frac{\partial u}{\partial x} = - \frac{1}{\rho} \frac{\partial P}{\partial x} + \frac{1}{\rho} I \tau_w \qquad \text{(momentum equation)}, \tag{2}$$

where $I = \dfrac{h+L_w}{h \cdot L_w}$, h = height of the cross-sectional area, and L_w = its width.

For this preliminary study, τ_w is included even though the flow is assumed to be isentropic. Results of computations indicate that its effect is small. The auxiliary equations are

$$P = \rho RT \qquad \text{(ideal-gas law)}, \tag{3}$$

and

$$c = c_o \left(\frac{P}{P_o} \right)^{\frac{\gamma-1}{2\gamma}} \qquad \text{(local sound speed)}. \tag{4}$$

where c_o and P_o are the ambient sound speed and pressure. Since $c^2 = \gamma RT$, $\frac{\partial \rho}{\partial x} = \frac{\rho}{\gamma P} \frac{\partial P}{\partial x}$ and $\frac{\partial \rho}{\partial t} = \frac{\rho}{\gamma P} \frac{\partial P}{\partial t}$, the final form of our differential equations describing the one-dimensional, compressible viscous nonsteady propagation of aerodynamic disturbances in any passageway of constant cross section is given by the following equations

$$\frac{\partial u}{\partial t} + u \frac{\partial u}{\partial x} + \frac{c^2}{\gamma P} \frac{\partial P}{\partial x} + \frac{I \cdot f}{2} u|u| = 0 \tag{5}$$

$$\frac{\partial P}{\partial t} + u \frac{\partial P}{\partial x} + \gamma P \frac{\partial u}{\partial x} = 0 \tag{6}$$

$$P = \rho RT \tag{3}$$

$$c = c_o \left(\frac{P}{P_o}\right)^{\frac{\gamma-1}{2\gamma}} \tag{4}$$

$$f = 0.0014 + 0.125 \left(\frac{\text{mean velocity} \times I}{\nu}\right)^{-0.32} \tag{7}$$

for laminar flow in smooth wall.

Strictly speaking, viscous term should not be included in the isentropic model. However, it may be regarded here as a perturbation. In subsequent discussions, this closed system of two partial differential equations and two algebraic equations (equations 3, 4, 5, 6, and 7) will be referred to as the "system."

The two equations, 5 and 6, are often referred to as a quasi-linear system since the coefficients of $\frac{\partial P}{\partial x}$ and $\frac{\partial u}{\partial x}$ depend on P and u but not on their derivatives. Furthermore, they constitute a hyperbolic system of which the existence and uniqueness of solution have been well-established for appropriate boundary and initial conditions.

Boundary and Initial Conditions

Initially, at t=0, the velocity and pressure are set equal to zero and atmospheric pressure everywhere, respectively.

There are only two boundary conditions prescribed. At the open-end (x=L), pressure (P(L,t)) is always equal to the ambient or atmospheric pressure (P_o). At the closed-end x=0, where combustion starts, one may prescribe either P(0,t) or u(0,t). If u(0,t) is prescribed and P(0,t) is calculated, then it simulates the situation where the flame has induced a velocity profile at x=0. The flame itself may be imagined to develop within a section behind x=0. Figure 1 illustrates this case where a growing hemispherical flame front induces a prescribed velocity history at x=0.

To use P(0,t) to compute u(0,t) corresponds to the case where an experimentally measured P(0,t) is prescribed. One must hasten to add that the portion of the experimentally measured P(0,t) used in this simulation should not contain information from the reflected signal as will be seen in a subsequent calculation; this situation is unavoidable in short galleries and leads to anomalous system histories.

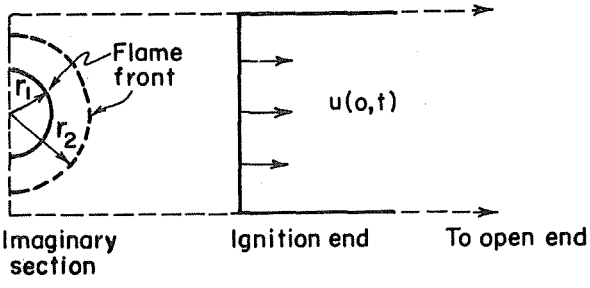

FIGURE 1. - Piston model.

Method of Characteristics

The method of characteristics (7, 12) in general works well for a

quasi-linear hyperbolic system of two first-order equations in two independent variables x and t. This method reduces the two partial differential equations to an equivalent system of four first-order ordinary-differential equations (4, 15-16):

$$\frac{du}{dt} + \frac{c}{\gamma P}\frac{dP}{dt} = -\frac{2 \cdot f}{D} u|u| \left[1-(\gamma-1)\frac{u}{c}\right], \tag{8}$$

$$\frac{dx}{dt} = u + c, \tag{9}$$

$$\frac{du}{dt} - \frac{c}{\gamma P}\frac{dP}{dt} = -\frac{2 \cdot f}{D} u|u| \left[1+(\gamma-1)\frac{u}{c}\right], \tag{10}$$

and

$$\frac{dx}{dt} = u - c. \tag{11}$$

Numerical Procedure

One numerical method commonly used consists of constructing a characteristic mesh from equations 8 through 11 and then obtaining the spatial distribution of the dependent variables at a fixed time through lengthy two-dimensional interpolations within the characteristic mesh (12, 14-15). However, in this study the method of Hartree (12) is followed, whereby one establishes a fixed grid as shown in figure 2, and at each cycle of the computation, all flow field variables are defined at all the mesh points at time t. To compute U(D, t + Δt) and (P(D, t + Δt), one constructs the C_+ and C_- characteristic using finite difference analogues of equations 9 and 11, and solves these equations using quadratic interpolation. This is equivalent to estimating the position RN and SN in terms of U and P at A, B, and C at the earlier time t. Subsequently, equations 8 and 10 are numerically integrated along these two curves. To insure that P and U at D are truly signals acoustically propagated from the points RN and SN, within the intervals [A,B] and [B,C], Δt is chosen so that $\Delta t \leq \frac{\Delta x}{|u|+C}$, when u is the largest of the three $|u(x-\Delta x,t)|$, $|u(x,t)|$, and $|u(x+\Delta x,t)|$. See appendix B for the detailed finite difference equations used.

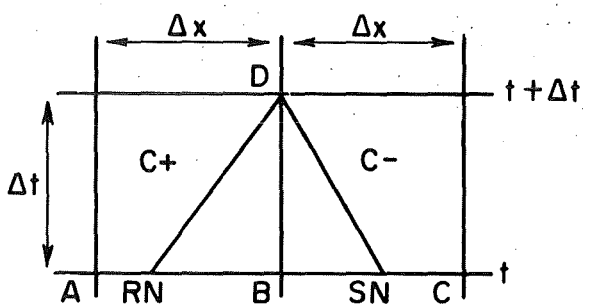

FIGURE 2. - Mesh for the method of characteristics.

RESULTS

The first application of the previous equations concerns a study of the aerodynamic disturbance created by a hemispherical flame developing at the end. This case involves prescribing the velocity profile at x = 0 induced by the growing hemispherical flame. Because of the velocity boundary prescription, this model will be subsequently referred to as the piston model. In the second

application, the pressure history at x = 0 is prescribed. Because pressure history boundary condition prescription is similar to that in a fan, this will be called the fan model. This is a semi-empirical model useful for extrapolating experimental histories to uninstrumented stations. In both cases, the authors examined the aerodynamics associated with flame propagating in a long cylindrical steel gallery, 1.22 m in diameter with the ignition end closed and the other end open (fig. 1).

Piston Model

The functional form for this velocity history for the first application is derived in the following manner. Assume that the flame front grows hemispherically with a burning velocity Su such that within a time interval δt, the flame advances into the unburned mixture a distance $Su \cdot \delta t$. Due to expansion of burned gas, the actual distance the flame travels relative to the gallery is, neglecting gas motion behind the flame front, given by $\delta r = Su \cdot E \cdot \delta t$. Since the flame speed is $S_f = E \cdot Su$, the volume δV_b of unburned gas displaced by the flame due to expansion is given by the expression

$$\delta V_b = \frac{1}{2} \cdot \frac{4\pi}{3} \left\{ (r+S_f \cdot \delta t)^3 - (r+Su \cdot \delta t)^3 \right\}$$

$$= \frac{2\pi}{3} \left\{ E^2 (E-1) \cdot Su^3 \cdot t^2 \cdot \delta t + O(\delta t^2) \right\} .$$

Therefore, the average gas velocity u at any cross section immediately ahead of the flame can be written as $u(0,t) = \lim_{\delta t \to 0} \frac{\delta V_b}{A \cdot \delta t} = \frac{2\pi}{3} E^2 (E-1) Su^3 \cdot \frac{t^2}{A}$. This is the velocity of the unburned gas prescribed at x = 0 during hemispherical flame growth. When the flame reaches the wall at time R/S_f, u(0,t) is set to a constant value for a short time to simulate translation of the hemispherical flame cap down the gallery. Following this, the flame extinguishes and the velocity is returned to zero. This model is equivalent to an accelerating piston driving air through a porous closed end.

In this first study the system parameters were

C_o	= 340	m sec^{-1}
γ	= 1.4	1
E	= 11.0	1
Su	= 1.524	m sec^{-1}
A	= 1.4192	m^2

and therefore

$$u(0,t) = \begin{cases} 8970.13\ t^2 & \text{for } 0 \le t \le 0.04 \\ 5 & \text{for } 0.04 \le t < 0.01 \\ 0 & \text{for } 0.1 \le t \end{cases} \qquad (12)$$

Furthermore, $P(50,t) = 14.57$ psi. The results of the calculation shown in figure 3 and figure 4 required 390 sec of central processor time on a Control Data Corp. (CDC) 6600 computer.[4] In these plots, $f = 0.0014 + \frac{0.125}{R_e^{0.32}}$. Two other cases were run with $f = 0$ and $f = 0.014 + \frac{1.25}{R_e^{0.32}}$.

Figure 3 shows the velocity histories at x=0-, 10-, 20-, 30-, 40-, and 50-m stations. The x=0-m station shows the velocity profile computed from equation 12. At t=0.04 sec, the flame reaches the gallery wall and the velocity is dropped to 5 m sec^{-1} and then to 0 m sec^{-1} after 0.1 sec. Figures 3 and 4 show the initial compression wave traveling toward the open end at the local sound speed c in the unburned gas; at the closed end, it is reflected as a rarefaction and returns back down the gallery. Since the 40-m station is within a distance to the open end less than the wavelength of the pulse (48 m), the trailing end of the pulse and the reflected portion of its leading edge superimpose appearing as two peaks not completely resolved, although at the 30-m station they are resolved. From the figures, one can see that the reflected pulse has a peak lower (by about 2.5%) than the incident pulse. Furthermore, the plateau in the pulse, which is sharp at inception, is a well-rounded shoulder at the 30-m station. By the time the pulse arrives at the 50-m station the third time, this feature has almost completely disappeared. This high-frequency filtering has been frequently observed in gallery experiments and will be discussed at greater length subsequently. Furthermore, the width of the pulse at x=0 is 0.10 sec and increases to 0.12 sec at the time of first reflection from the open end and further increases to 0.15 sec at the next reflection from the open end. At this time, wavelength of the pulse is equal to the length of the gallery (50 m), and it will not get any larger during subsequent reflections. These observations will be discussed later in this report. Although the viscous forces will eventually dissipate these disturbances, its width will not change after its wavelength reaches the gallery length. Elongation of the pulse wavelength with distance of travel is a quadratic function of the traveltime.

The Mach lines drawn in figure 3 corresponding to ambient sound speed in the unburned gas (340 m sec^{-1}) follows the leading edge of the pulse as expected. Although the local sound speed at the pressure peak differs from this by 2.3 m sec^{-1}, the effect of this small increase in sound speed is not perceptible in the plots. This explains why minimal steepening of the pressure pulses occurs in these plots. This is not true for pulses with higher pressure, for example, greater than 10 psi. However, even in this case, the

[4] Reference to specific products does not imply endorsement by the Bureau of Mines.

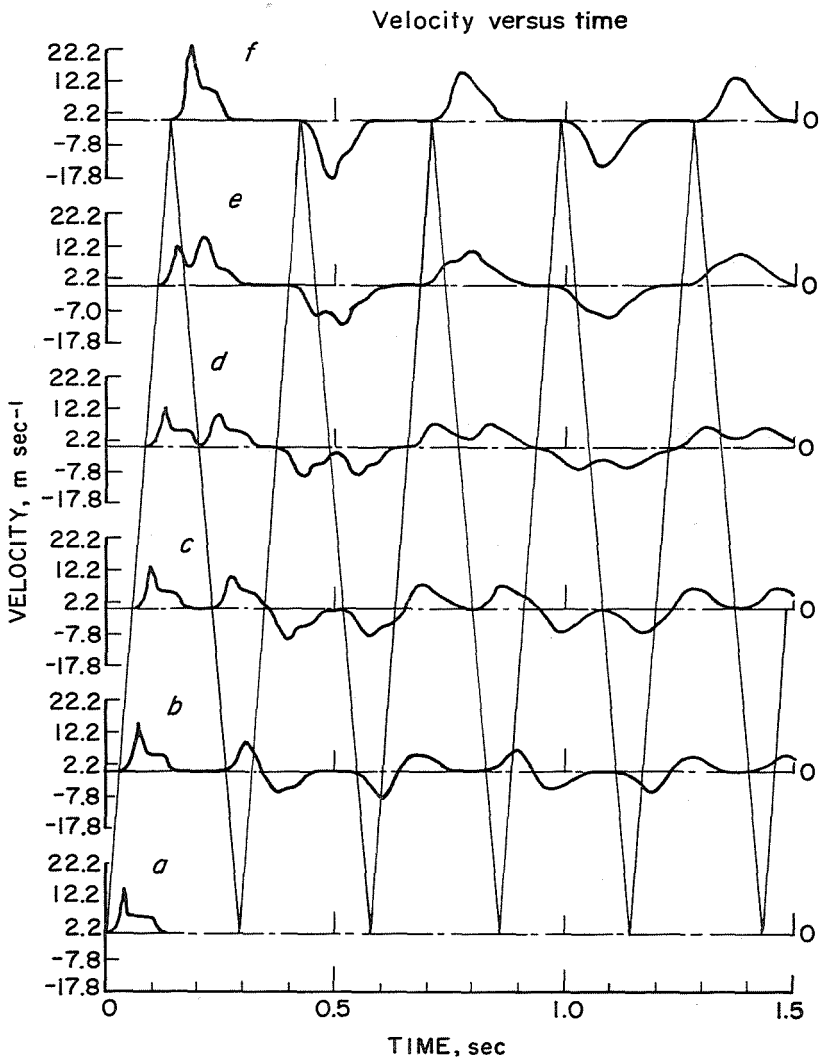

FIGURE 3. - Velocity histories at *(a)* 0-, *(b)* 10-, *(c)* 20-, *(d)* 30-, *(e)* 40-, and *(f)* 50-m stations.

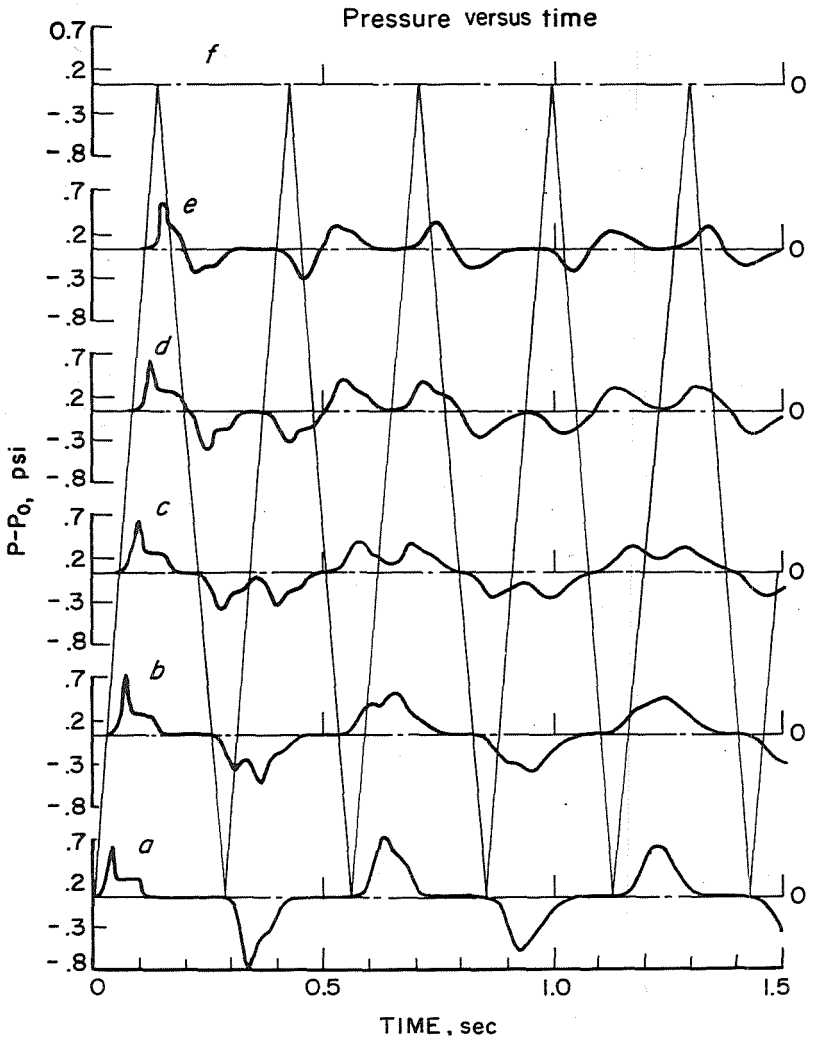

FIGURE 4. - Pressure histories at *(a)* 0-, *(b)* 10-, *(c)* 20-, *(d)* 30-, *(e)* 40-, and *(f)* 50-m stations.

slope of the incident velocity pulses steepens from approximately 25 m sec^{-2} at x=0 to 39 m sec^{-2} at the open end.

Figure 4 shows the pressure histories at various stations. In this case, the reflection of the pressure pulse from the open end causes phase reversal but conserves phase upon reflection from the closed end. Both of these are in accordance with elementary acoustics. Note also that the pressure amplitude decreases with distance of travel as was seen in the velocity histories. Furthermore, the pressure and velocity profiles form a complementary pair to the extent that given one the qualitative features of the other can be deduced. For instance, the pressure profile at the 40-m station is the same as velocity profile at the 10-m station except for a phase shift of 0.147 sec. Similarly, the pressure profile at 30 m is similar to that of velocity at 20-m station with the same phase shift. This relationship can be summarized by the following expression: $P(x,t)=c(x,t)\ u(L-x,\ t\pm0.147)$ where c is a weak function of t. This relationship is due to the geometry and boundary conditions. With regard to the boundary condition, a similar effect is produced by the open end and the closed end on pressure and velocity, respectively. The phase shift of 0.147 sec is precisely the time for a pulse to travel a distance of 50 m at a speed of 340 m sec^{-1}.

The results of this example shows favorable qualitative agreement with the experimental observations in the 50-m flame gallery. For instance, compare plot e of figure 4 with measured history in figure 6. The qualitative differences are due primarily to the presence of flame in the experiments and the different aerodynamic characteristics between the cold and hot gases.

Computer runs were made with several different values of the friction factor (0.0, 0.0014, 0.014), but the use of different values resulted in a maximum difference of only 0.1% to 0.5% in the velocity histories and less in the pressure histories as noted in reference 3 (p. 31), lending justification to an isentropic description. Therefore, it is concluded that if these wall friction factors are reasonable, wall drag is a negligible effect.

Fan Model

In the second study in which the measured pressure history at x=0 m provides the boundary conditions at the closed end, the pressure history contains the net effect of combustion and environment.

To illustrate this approach, the pressure and velocity records from test 79, using the 50-m flame gallery, were selected (17). In this experiment, pressure transducers and hot-wire anemometers were placed at distances 0, 8.2, 16.6, 24.6, 32.6, and 41 m from the closed end (ignition) of the gallery. A pocket of 8.4% natural gas/air mixture filling the first section of the closed end was ignited, and the flame propagated toward the open end. Corresponding to this situation, the boundary conditions at x=0 were specified as follows: $P(0,t)$ = (experimental pressure profile), $0\leq t\leq0.38$ sec and $u(0,t)=0$ for $t>0.38$ sec. At x=50 m, $P(50,t)=P_o$. Using equations 8 through 11 and these boundary and initial conditions, the velocity and pressure histories were then computed at points corresponding to those locations having measuring devices.

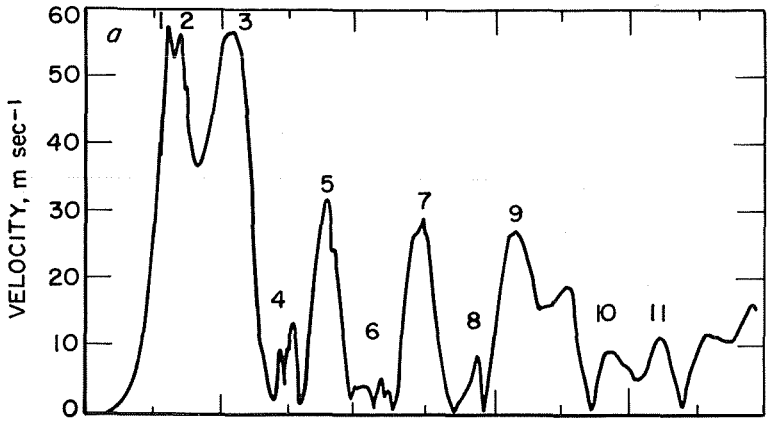

FIGURE 5. - Absolute velocity history measured at the 24.6-m station.

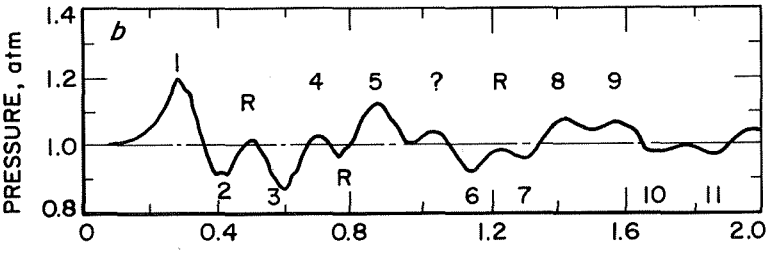

FIGURE 6. - Pressure history measured at 41.0-m station.

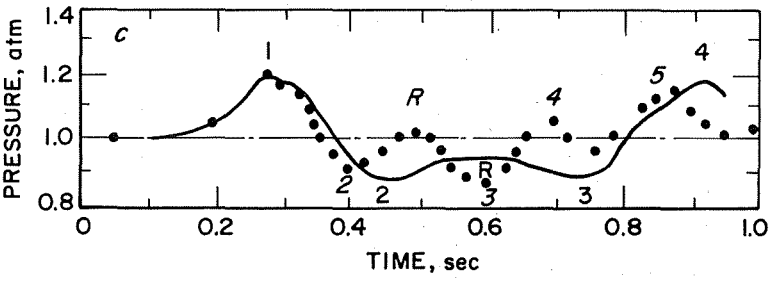

FIGURE 7. - Calculated pressure history at 40-m station with c_o=340 m sec^{-1} (dots represent experimental data).

Figure 5 shows the absolute velocity profile measured at the 24.6-m station, and figure 6, the pressure history measured at 41.0-m station. Because the air velocity is measured with single hot wires, only the absolute velocity is recorded. The flow direction was determined by means of a second hot wire provided with an appropriate shield for recording flow direction.

In the first solution, the calculation used a value of 340 m sec^{-1} for the ambient sound (c_o) corresponding to an air temperature of about 300 K. A comparison of the measured and calculated pressure history at 41.0 m is shown in figure 7. The figure shows that the histories are similar except that the calculated history appears to be compressed in time. The compression can be remedied by increasing the ambient sound speed to 420 m sec^{-1}, corresponding to an average gas temperature of 439 K. This is not unreasonable in view of the presence of the hot-burned-gas volume present in the experiments. The results of the calculation using this sound speed are shown in figures 8 and 9.

An examination of the calculated and measured pressure histories shown in figure 8 shows reasonable qualitative agreement to the extent that the shape of the histories are similar. This is most evident at the 41-m station where the majority of the peaks are resolved, although the calculated pressure history consistently overestimates the measured values. This difficulty results from being unable to exactly duplicate both the measured pressure and velocity at the closed end simultaneously during the first 0.4 sec. Since in solving the partial differential equations (PDE's) only one of the variables (p or v) can be prescribed at the closed end, the other variable must assume a value

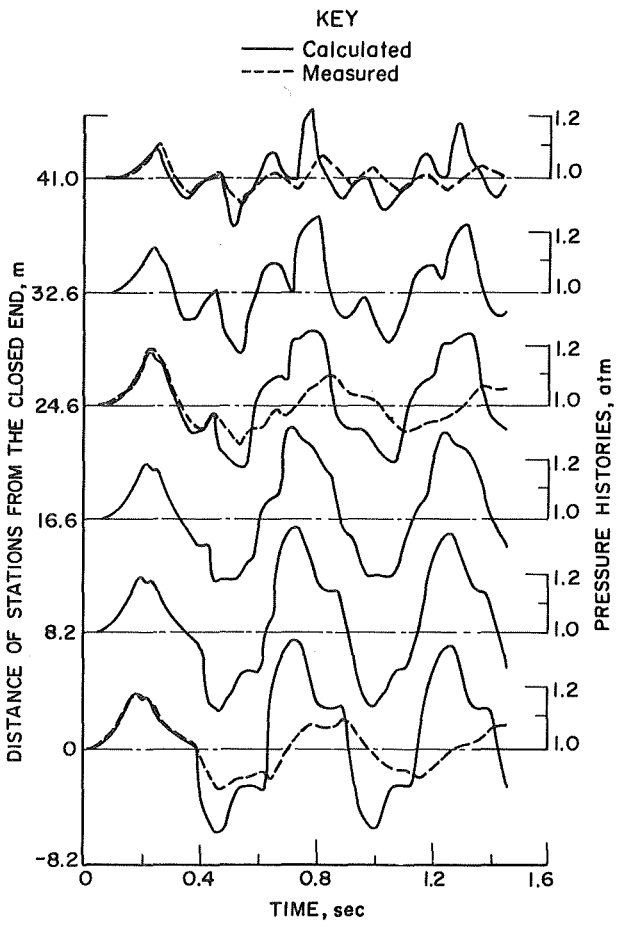

FIGURE 8. - Computed pressure histories for c_o=420 m sec^{-1}.

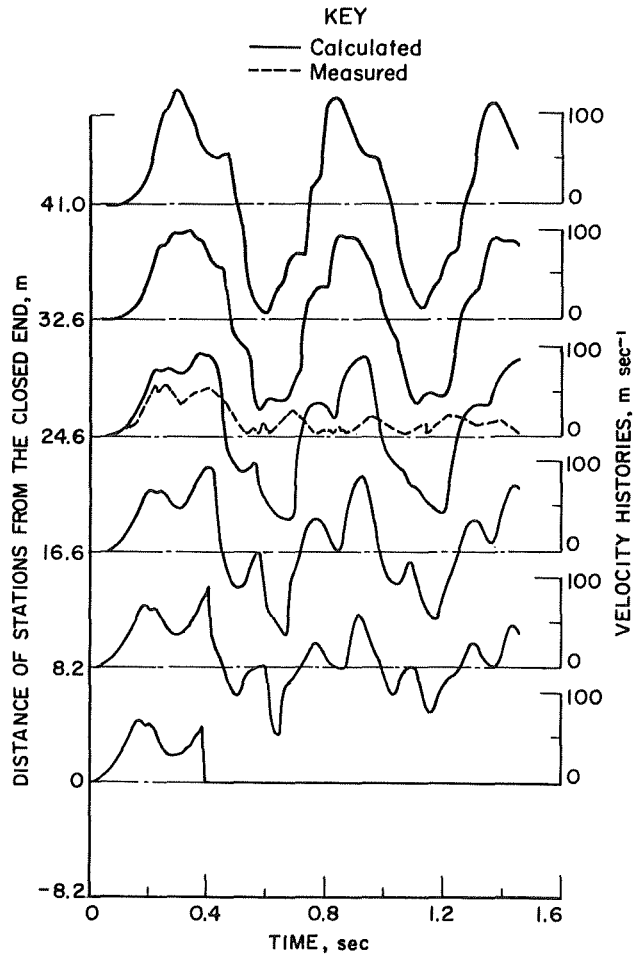

FIGURE 9. - Computed velocity histories for c_o=420 m sec^{-1}.

dictated by the solution of the PDE. Unfortunately, at 0.38 sec, when the measured pressure reached its ambient value, the calculated velocity as seen from the 0.0-m station record in figure 9 has attained a value of about 70 m sec^{-1}. Since this boundary is closed by definition, there is no alternative but to set the velocity equal to zero after 0.38 sec, which is what has been done in the calculation. Unfortunately, as seen in the 0.0-m station history of figure 9, this resulted in an abrupt drop in the velocity from 70 to 0 m sec^{-1}, which in turn caused a corresponding abrupt drop in the pressure at the 0-m station record at 0.38 sec. Figure 9 shows more clearly the cause of this phenomena, namely, the rarefaction created at the open end by reflection of the initial compression wave returns to the closed end before the pressure is returned to zero causing a minimum in the velocity history at 0.28 sec followed by the subsequent increasing velocity; up to 0.28 sec, the pressure and velocity were in phase. If the gallery had been longer than 79.8 m (=0.38 sec X 420 m sec^{-1}/2), rather than 50 m, the leading edge of the reflected pulse would have arrived at the closed end after the pressure at the face had returned to ambient and the velocity had returned to zero. In that case, the solution would not have experienced the discontinuity in the velocity history, and the velocity and pressure histories at the face would have

remained in phase. The abrupt drop in the calculated pressure at 0.38 sec causes this pressure to fall twice as low as it should, and this exaggerated pressure drop continues to manifest itself in the remainder of the calculated pressure history as exaggerated peaks and valleys.

The agreement between the measured and calculated velocity histories has the same problem on the pressure histories; namely, the presence of the anomalous distrubance generated at 0.38 sec presents quantitative agreement although the qualitative features are in reasonable agreement to the extent that the maxima and minima evident in the pressure history occur in corresponding sequences.

It is unfortunate that no measured histories are available in which the flame extinguished prior to the arrival of the first reflected disturbance.

Although quantitative agreement was lacking, it is still believed that this approach will find general use in extending measured history variables to uninstrumented stations in those situations where the ratio of the gallery length to wavelength of the initial disturbances is greater than one-half.

It is clear from the study that sound speed and gallery length are important factors in determining the system history. The code provides a means of using experimentally measured histories obtained in laboratory equipment; for example, a 50-m-long gallery to calculate similar histories in full-scale facilities. Of course, the phenomena of the initial growth of flame also plays an important role; however, it is not a decisive one as far as the wave forms are concerned.

Further Properties of Compressible Flow in a Single-Entry Mine

It has been observed (17) experimentally that pressure and velocity pulses broaden with time, asymmetrically approaching a sinusoidal history corresponding to the first fundamental resonant mode of the gallery. To illustrate this point, an examination was made of the aerodynamic history of the 50-m flame gallery for which the period of the first fundamental mode (2 Hz) is 0.5 sec if the local sound speed is 400 m sec^{-1}. Consider the following three cases:

Case 1 ($T_1 < 0.5$)

$$u(0,t) = \begin{cases} 523.59\ t & \text{for } 0 \le t \le 0.038 \text{ sec} \\ -523.59\ t + 40 & \text{for } 0.038 \le t \le 0.24/\pi \\ 0 & \text{for } 0.076 < t \end{cases}$$

$$P(50,t) = P_o$$

where T_1 is the period of the wave for the first case. Here $0.076 = 0.24/\pi$ is selected to insure that the period of the initial disturbance is not a submultiple of the period of the gallery.

Case 2 ($T_2 = 2\ T_1$)

$$u(0,t) = \begin{cases} 130.90\ t & \text{for } 0 \le t \le 0.24/\pi \\ -130.90\ t + 40 & \text{for } 0.24/\pi \le t \le 0.48/\pi \\ 0 & \text{for } 0.48/\pi < t \end{cases}$$

$$P(50,t) = P_o$$

Case 3 ($T = 0.5$)

$$u(0.t) = \begin{cases} 160\ t & \text{tor } 0 \le t \le 0.125 \\ -160\ t + 40 & \text{for } 0.125 \le t \le 0.250 \\ 0 & \text{for } 0.250 < t \end{cases}$$

$$P(50,t) = P_o$$

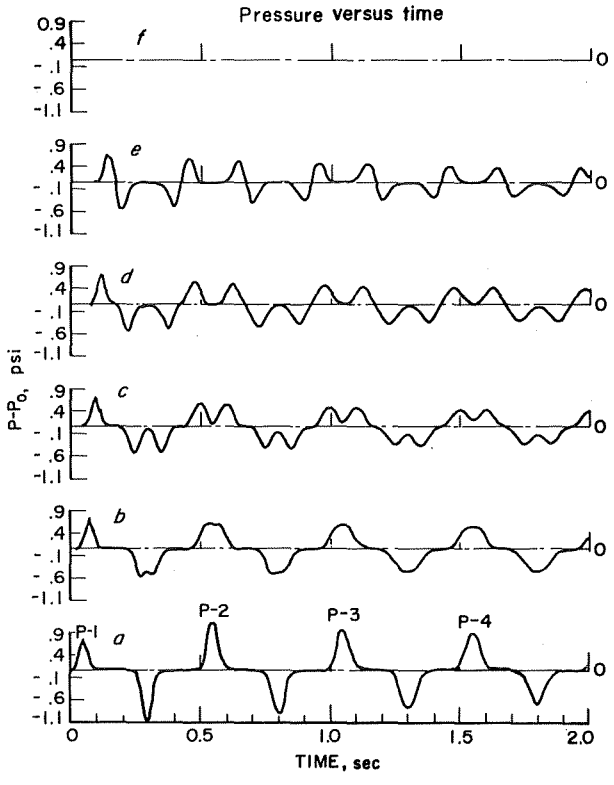

FIGURE 10. - Pressure histories at *(a)* 0-, *(b)* 10-, *(c)* 20-, *(d)* 30-, *(e)* 40-, and *(f)* 50-m stations for case 1.

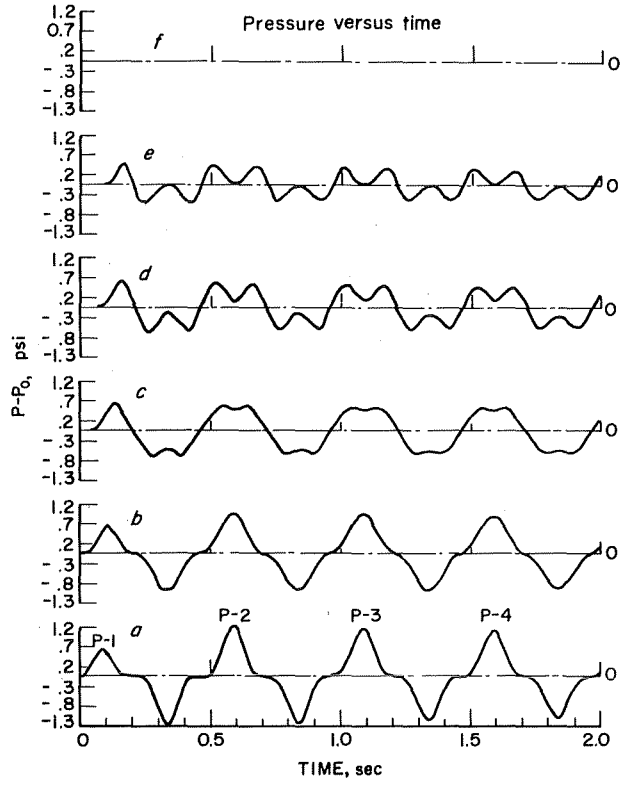

FIGURE 11. - Pressure histories at *(a)* 0-, *(b)* 10-, *(c)* 20-, *(d)* 30-, *(e)* 40-, and *(f)* 50-m stations for case 2.

Case 3 corresponds to the situation where the duration of excitation is exactly one-quarter the gallery length, corresponding to half the period of the fundamental frequency. Pressure histories for these three cases are presented in figures 10 through 12. Consider the first wave form (labeled P1) at the face station as the input signal to the system and the remaining pulses (labeled P2, P3, and P4) as outputs. The broadening of the pulses, which can most readily be seen in the face station records, is calculated by measuring changes in the width of the pulses at half height. In addition to the usual pressure doubling in the face station between the first and second pulses, we also see that the peak pressure of the successive pulses decreases. As table 1 shows, the closer the input pulse frequency is to the fundamental gallery frequency (2 Hz), the smaller the rate of change of the pulse characteristic. In all cases, the impulse remains essentially constant as expected in a nondissipative system. The small deviation from a constant impulse is attributed to the truncation error of the numerical integration rather than to any physical phenomena.

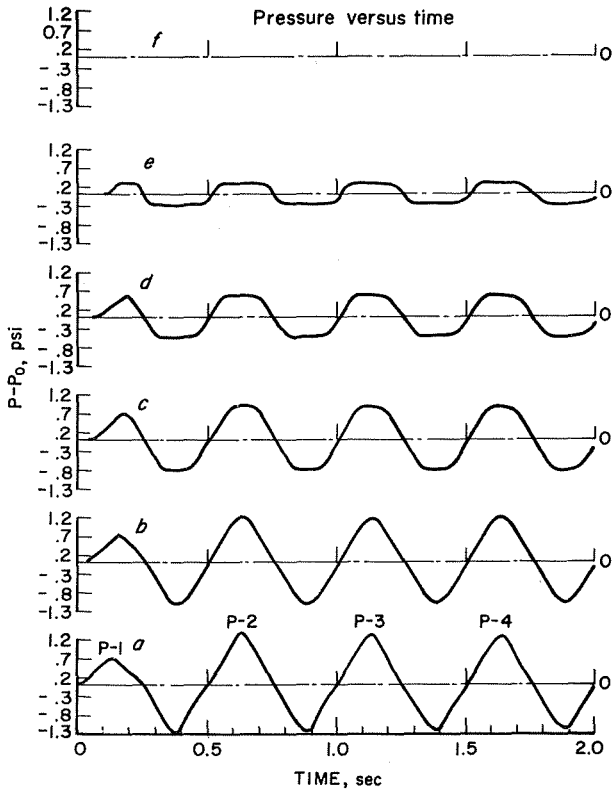

FIGURE 12. - Pressure histories at *(a)* 0-, *(b)* 10-, *(c)* 20-, *(d)* 30-, *(e)* 40-, and *(f)* 50-m stations for case 3.

TABLE 1. - Changes in peak pressure and peak half-width percentages

	$\frac{P2-2XP1}{2XP1} \times 100$, %	$\frac{P3-P2}{P2} \times 100$, %	$\frac{P4-P3}{P3} \times 100$, %
Peak pressure above ambient:			
Case 1.....	-25.4	-23	-10.6
Case 2.....	-11.7	-6	-5.7
Case 3.....	-5.7	-3.8	-3.0
Half width:			
Case 1.....	+64.5	+18.7	+16
Case 2.....	+28.5	+4.6	+4.3
Case 3.....	+6.3	+3.0	+2.9

TABLE 2. - Impulses, lb_f sec

	Impulse of P1	Impulse of P2	Impulse of P3	Impulse of P4
Case 1.....	0.056	0.057	0.057	0.057
Case 2.....	.112	.116	.115	.115
Case 3.....	.184	.188	.187	.187

The phenomena described in the previous paragraph is a result of the fact that the passageway of a mine network behaves like a low-pass filter. As aerodynamic disturbances traverse various mine sections, the spectral energies of the disturbances are shifted toward those frequencies corresponding to the various system resonances. To illustrate this point, a spectral analysis (18) was carried out on pulses P1 and P3 of case 2 and case 3. Recall that P1 of case 2 corresponds to a signal whose predominant signal is 3.29 Hz, and P1 of case 3 is predominately 2 Hz. Figures 13A and 13B show amplitude versus frequency plots for P1 and P3 of case 2, and indeed, figure 13A shows a strong peak at 3.29 Hz for P1. After the P1 pulse has traversed the gallery length five times becoming pulse P3, figure 13B shows that its predominant energy component has shifted to that at the first fundamental frequency of the gallery, namely, 2 Hz.

In case 3, however, P1 already has a predominant energy component at 2 Hz (fig. 14A). After five traversals of the gallery length becoming P3, figure 14B shows no major changes in its spectra (fig. 14B), showing again that pulses with the bulk of its energy in the first fundamental mode undergo minimal changes during multiple traversals of the gallery. It seems reasonable to to conclude, therefore, that to minimize pressure damage in coal mine disasters a coal mine should be designed to distribute the wave energy over a broad spectral range.

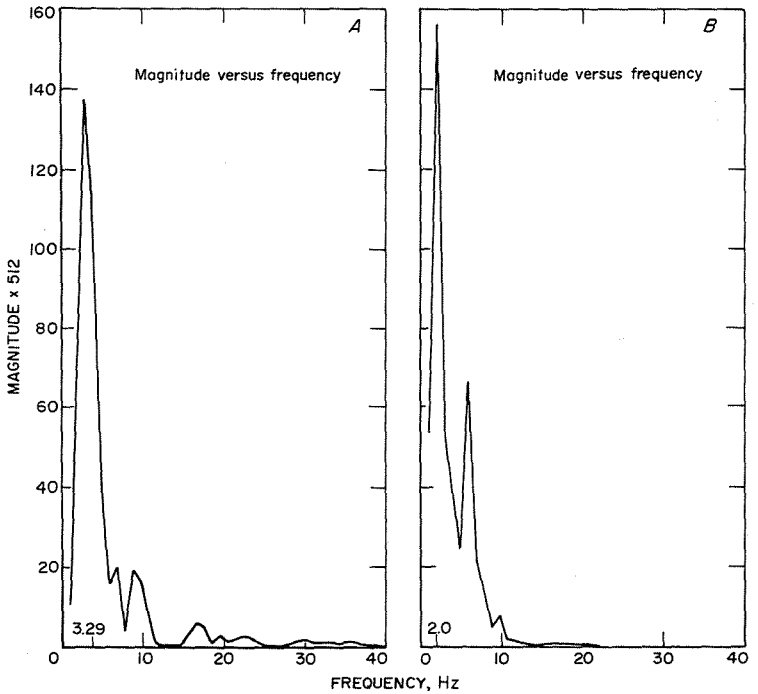

FIGURE 13. - Amplitude versus frequency plots for *(A)* P1 and *(B)* P3 of case 2.

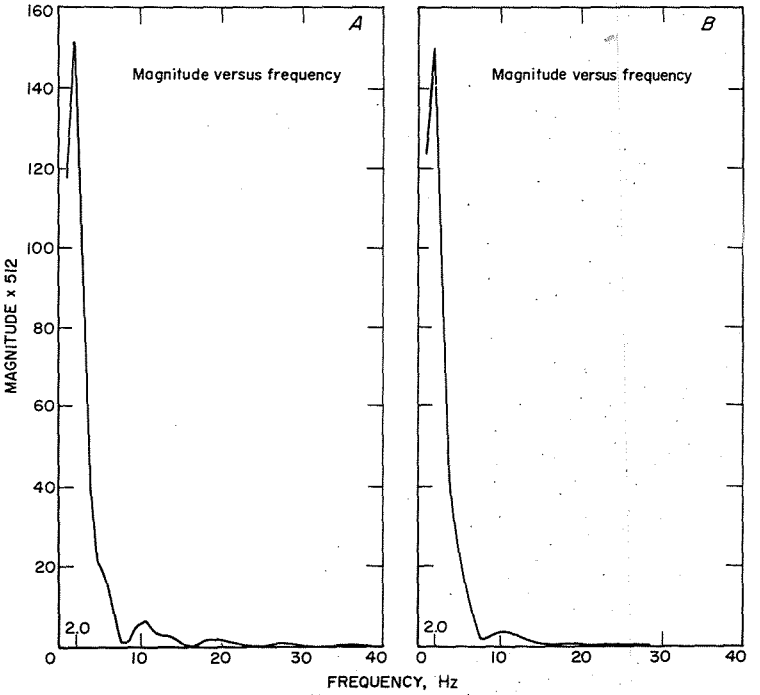

FIGURE 14. - Amplitude versus frequency plots for *(A)* P1 and *(B)* P3 of case 3.

CONCLUSIONS

The unsteady one-dimensional compressible flow equations were solved using the method of characteristics to determine the feasibility of extending this technique to study the transient aerodynamic response characteristics of the networks of coal mine passageways. The computation for a single passageway required about 150 sec of central processor time on a CDC-6600 computer for each second of real time simulated and each 100 ft of passageway. For a coal mine room-and-pillar system 1,000 ft deep with eight entries having 100-ft centers and crosscuts with similar separation, the solution would require 1.8 sec of real time to study the aerodynamic history for a single cycle.[5] Since the area contains a total of 14,000 ft (140 100-ft sections) of passageway, it is estimated that the method of characteristic would require 1.8 * 140 * 150 = 21,000 sec (5.8 hr) of computer time on a CDC-6600. Obviously, some improvement in the computer time required can be obtained at a sacrifice in accuracy by using larger finite difference increments in both time and space. No attempt has been made either to optimize the computer program or determine the accuracy resulting from the use of larger finite difference increments. It is estimated that most likely a factor of two or three reduction in run time can be realized when both these factors are taken into consideration.

This modeling technique can be used as a tool to extend the measured velocity and pressure histories to uninstrumented stations. Although quantitative agreements especially for the latter may be off, qualitative agreement is very good. It can provide such information as the optimum locations for a passive water barrier, total impulse or a temporary stoppage, etc. In the case where hot-wire measurements of velocities provide no indication of the direction of flow, this modeling technique can provide such complementary information. This modeling technique also may be used to examine the filtering characteristics of entryways.

[5]A single cycle is the time necessary for a sound wave to travel twice the longest dimension of the area.

REFERENCES

1. Artingstall, G. On the Relation Between Flame and Blast in Coal-Dust Explosion. Safety in Mines Res. Establishment, England, Rept. No. 204, September 1961, 35 pp.

2. Artingstall, G., and T. C. Corlett. The Effect of Pressure Waves on the Propagation of Dust Explosions. Safety in Mines Res. Establishment, England, Res. Rept. No. 238, December 1965, 17 pp.

3. Chi, D. N., and H. E. Perlee. Mathematical Study of a Propagating Flame and Its Aerodynamics in a Coal Mine Passageway. BuMines RI 7908, 1974, 51 pp.

4. Courant, R., and K. O. Friedrichs. Supersonic Flow and Shock Waves. Interscience Publishers, Inc., New York, 1948, pp. 40-48.

5. Cybulski, W. B. Correlation Between the Flame Velocity and the Dynamic Pressure Under the Conditions of Very Weak Coal-Dust Explosions. Bulletin De L'Academi Polonaise Des Sciences, v. 28, No. 12, 1970, pp. 9-17.

6. Ferri, A. (ed.). Fundamental Data Obtained From Shock-Tube Experiments. Pergamon Press, New York, 1961, 415 pp.

7. Issa, R. I., and D. B. Spalding. Unsteady-One-Dimensional Compressible Frictional Flow With Heat Transfer. J. Mech. Eng. Sci., v. 14, No. 6, 1972, pp. 365-369.

8. Jones, H. Accelerated Flames and Detonation in Gases. Proc. Royal Soc., (London), v. A248, 1958, pp. 333-349.

9. Laderman, A. J., and A. K. Oppenheim. Initial Flame Acceleration in an Explosive Gas. Proc. Royal Soc. (London), v. A268, 1962, pp. 153-180.

10. Lebecki, K. Research on the Theory of Dust Explosions. Safety in Mines Res. Establishment, England, Trans. No. 5489, 1967, 20 pp.

11. Liebman, I., and J. K. Richmond. Suppression of Coal Dust Explosion by Passive Barrier in a Single-Entry Mine. BuMines RI 7815, 1974, 34 pp.

12. Lister, M. The Numerical Solution of Hyperbolic Partial Differential Equations by the Method of Characteristics. In Mathematical Methods for Digital Computers, v. 1, ed. by A. Ralston and H. Wilf. John Wiley & Sons, Inc., New York, 1967, pp. 165-179.

13. Oppenheim, A. K. On the Dynamics of the Development of Detonation in Gaseous Medium. Archiwum Mechniki Stosowanej, v. 2, No. 16, 1964, pp. 403-424; available from National Technical Information Service, Springfield, Va., AD 622 842.

14. Richtmyer, R. D. Difference Methods for Initial Value Problems. Interscience Publishers, Inc., New York, 1964, 238 pp.

15. Rudinger, G. Wave Diagrams for Unsteady Flow in Ducts. Van Nostrand Co., Inc., New York, 1955, 278 pp.

16. Shapiro, A. H. The Dynamics and Thermodynamics of Compressible Fluid Flow. Ronald Press, New York, v. 2, 1954, 1185 pp.

17. Singer, J. Private Communications. Available for consultation at the Bureau of Mines, Pittsburgh Mining and Safety Research Center, Pittsburgh, Pa.

18. Webb, C. Practical Use of the Fast Fourier Transform (FFT) Algorithm in Time-Series Analysis. Report ARL-TR-7022 (AD-713166), University of Texas, Austin, Tex., June 22, 1970, 205 pp.

APPENDIX A.--DERIVATION OF THE MOMENTUM EQUATIONS WITH FRICTION

A. Ferri has presented (6) a detailed account of the averaging procedure of the flow fields over a cross-sectional area; however, he does not include the wall friction term. In what follows, we will attempt to fill this gap.

Let $u(x, y, z)$, $v(x, y, z)$, and $w(x, y, z)$ be the three components of the velocity, $\vec{w}$, in the x, y, and z directions. Let $X(x, y, z)$, $Y(x, y, z)$, and $Z(x, y, z)$ be the three components of body forces. The momentum equations can then be expressed as follows:

$$\rho \frac{Du}{Dt} = X - \frac{\partial P}{\partial x} + \frac{\partial}{\partial x}\left[\mu\left(2\frac{\partial u}{\partial x} - \frac{2}{3}\operatorname{div}\vec{w}\right)\right] + \frac{\partial}{\partial y}\left[\mu\left(\frac{\partial u}{\partial y} + \frac{\partial v}{\partial x}\right)\right] + \frac{\partial}{\partial z}\left[\mu\left(\frac{\partial w}{\partial x} + \frac{\partial u}{\partial z}\right)\right], \qquad \text{A-1}$$

$$\rho \frac{Dv}{Dt} = Y - \frac{\partial P}{\partial y} + \frac{\partial}{\partial y}\left[\mu\left(2\frac{\partial v}{\partial y} - \frac{2}{3}\operatorname{div}\vec{w}\right)\right] + \frac{\partial}{\partial x}\left[\mu\left(\frac{\partial u}{\partial y} + \frac{\partial v}{\partial x}\right)\right] + \frac{\partial}{\partial z}\left[\mu\left(\frac{\partial v}{\partial z} + \frac{\partial w}{\partial y}\right)\right], \qquad \text{A-2}$$

and

$$\rho \frac{Dw}{Dt} = Z - \frac{\partial P}{\partial x} + \frac{\partial}{\partial z}\left[\mu\left(2\frac{\partial w}{\partial z} - \frac{2}{3}\operatorname{div}\vec{w}\right)\right] + \frac{\partial}{\partial x}\left[\mu\left(\frac{\partial w}{\partial x} + \frac{\partial u}{\partial z}\right)\right] + \frac{\partial}{\partial y}\left[\mu\left(\frac{\partial v}{\partial z} + \frac{\partial w}{\partial y}\right)\right]. \qquad \text{A-3}$$

Let the flame gallery be so oriented that the longitudinal direction is in the x direction; then assumptions 1, 2, 3, 4, and 5 of the section "Assumptions" imply that

(1) $u = u(x,y,z,t)$; $v/u \ll 1$, $w/u \ll 1$;

(hence negligible)

(2) $X = Y = Z = 0$

(3) $\tau_{xy} = \mu \left.\frac{\partial u}{\partial y}\right|_{wall} = \tau_w$ (a constant)

$\tau_{xz} = \mu \left.\frac{\partial u}{\partial z}\right|_{wall} = \tau_w$

(4) $\frac{\partial P}{\partial y} = \frac{\partial P}{\partial z} = 0$; and finally,

(5) $\mu \frac{\partial^2 u}{\partial x^2} \ll \frac{\partial P}{\partial x} \Longrightarrow \mu \frac{\partial^2 u}{\partial x^2}$ is negligible.

With these assumptions, A-1, A-2, and A-3 can be reduced to

$$\rho \frac{Du}{Dt} = - \frac{\partial P}{\partial x} + \mu \frac{\partial^2 u}{\partial y^2} + \mu \frac{\partial^2 u}{\partial z^2} \qquad \text{A-4}$$

and

$$\frac{\partial^2 u}{\partial x \partial y} = \frac{\partial^2 u}{\partial x \partial z} = 0 \; . \qquad \text{A-5}$$

Let $\rho = \overline{\rho}(x,t) + \epsilon \cdot a(x,y,z)$

$P = \overline{P}(x,t) + \epsilon \cdot b(x,y,z)$

$U = \overline{u}(x,t) + \epsilon \cdot c(x,y,z)$

where

$$\int_A a dA = 0, \quad \int_A b dA = 0, \quad \int_A c dA = 0 \; ,$$

$$\overline{\rho} = \int_A \rho dA/A, \quad \overline{P} = \int_A P dA/A, \quad \overline{u} = \int_A u dA/A$$

and ϵ = a small number.

Now, if one integrates (A-4) over A and throws away terms of second order in ϵ, one gets

$$\overline{\rho} \frac{D\overline{u}}{Dt} = - \frac{\partial \overline{P}}{\partial x} \pm \frac{1}{A} \int_A \mu \frac{\partial^2 u}{\partial y^2} dA + \frac{1}{A} \int_A \mu \frac{\partial^2 u}{\partial z^2} dA \; . \qquad \text{A-6}$$

Consider the first integral

$$\frac{1}{A} \int_A \mu \frac{\partial^2 u}{\partial y^2} dA = \frac{1}{A} \iint_A \mu \frac{\partial^2 u}{\partial y^2} dy dz = \frac{1}{A} \int_{-h}^{h} \mu \frac{\partial u}{\partial y} \Bigg|_{-L}^{L} dz$$

$$= \frac{1}{A} \tau_w \; (2 \cdot h) \; . \qquad \text{A-7}$$

Similarly

$$\frac{1}{A} \int_A \mu \frac{\partial^2 u}{\partial z^2} dA = \frac{1}{A} \tau_w \; (2 \cdot L) \; . \qquad \text{A-8}$$

Note that A=2h×2L; hence, we define $I = \frac{2L}{A} + \frac{2h}{A} = \frac{h+L}{h \cdot L}$.

Thus, A-6 takes on the final form

$$\overline{\rho} \frac{D\overline{u}}{Dt} = - \frac{\partial \overline{P}}{\partial x} + I \cdot \tau_w \; . \qquad \text{A-9}$$

It is further assumed that the effect of wall friction can be expressed in terms of the conventional pipe friction coefficient f defined by

$$f = - \frac{\tau_w}{\frac{1}{2}\bar{\rho}\bar{u}^2} \qquad \text{A-10}$$

one obtains

$$\tau_w = - \frac{f}{2} \bar{\rho} \cdot \bar{u}^2 \ . \qquad \text{A-11}$$

Hence,

$$\bar{\rho} \frac{D\bar{u}}{Dt} = - \frac{\partial \bar{P}}{\partial x} - \frac{I}{2} f \bar{\rho} \bar{u}^2 . \qquad \text{A-12}$$

In this paper we then replace $\bar{\rho}$, $\bar{u}$, $\bar{P}$ by ρ, u, P with the understanding that ρ, u, P actually represents averaged quantities. With this interpretation A-12 is then precisely the governing equation 2.

APPENDIX B.--DERIVATIONS OF THE FINITE DIFFERENCE EQUATIONS

In the following discussions, PRN, PSN, URN, USN, CRN, CSN are the values of P, U, and C at the points RN, SN (fig. 2). The superscipts k and k + 1 refer to the time levels $k\cdot\Delta t$ and $(k+1)\Delta t$ while the subscripts n, (n + 1) and (n - 1) refer to the locations $n\cdot\Delta x$, $(n + 1)\Delta x$, and $(n - 1)\Delta x$.

The finite difference analogue of equations can be written as

$$\frac{U_n^{k+1} - URN}{\Delta t} + \frac{CRN}{PRN}\frac{(P_n^{k+1} - PRN)}{\Delta t} + \frac{I\cdot f}{2}\cdot URN|URN| = 0 \qquad \text{B-1a}$$

$$\frac{XN - RN}{\Delta t} = URN + CRN \qquad \text{B-1b}$$

$$\frac{U_n^{k+1} - USN}{\Delta t} - \frac{CSN}{PSN}\frac{(P_n^{k+1} - PSN)}{\Delta t} + \frac{I\cdot f}{2} USN\cdot|USN| = 0 \qquad \text{B-1c}$$

$$\frac{XN - SN}{\Delta t} = USN - CSN \qquad \text{B-1d}$$

Also needed are

$$CRN = \frac{C_o}{\gamma}\left(\frac{PRN}{P_o}\right)^{\frac{\gamma-1}{\gamma}} \qquad \text{B-2}$$

and

$$CSN = \frac{C_o}{\gamma}\left(\frac{PSN}{P_o}\right)^{\frac{\gamma-1}{\gamma}} \qquad \text{B-3}$$

With B-1b and B-1D, B-1a and B-1c may be written as

$$C_+ : (PRN)U_n^{k+1} + (CRN)P_n^{k+1} = PRN(URN + CRN) - \frac{I\cdot f}{2} PRN\cdot\Delta t\cdot URN|URN| \qquad \text{B-4a}$$

$$C_- : (PSN)U_n^{k+1} - (CSN)P_n^{k+1} = PSN(USN - CSN) - \frac{I\cdot f}{2} PSN\cdot\Delta t\cdot USN|USN| . \qquad \text{B-4b}$$

Note that if XN is a boundary point, then only one of the previous equations is applicable. For instance, at X=0, only B-4b is applicable. Since there are two unknowns, one boundary condition must be specified. Similarly, one must specify only one boundary condition at the open end X=L. This is an instance where a numerical algorithm illuminates the choice and need of appropriate boundary condition to yield a well-defined problem. Away from the

boundary, at any point X = n Δx one has (by solving B-4a and B-4b simultaneously)

$$P_n^{k+1} = \frac{(PRN)(PSN)\left\{(URN-USN+CRN+CSN) + \frac{I\cdot f}{2}\Delta t(USN|USN| - URN|URN|)\right\}}{(PSN)(CRN) + (PRN)(CSN)} \qquad B\text{-}5$$

$$U_n^{k+1} = \left(\frac{CSN}{PSN}\right) P_n^{k+1} + (USN-CSN) - \frac{I\cdot f}{2}\Delta t\ USN|USN| \qquad B\text{-}6$$

in which PSN, PRN, USN, URN, CRN, CSN are still unknown.

By linear interpolation (fig. 2) and by using equations B-1a and B-1d, we set

$$USN = \frac{(1-\theta\cdot CSN)U_n^k + \theta\cdot CSN\cdot U_{n+1}^k}{1 + \theta(U_n^k - U_{n-1}^k)} \qquad B\text{-}7a$$

$$URN = \frac{(1-\theta\cdot CRN)U_n^k + \theta\cdot CRN\cdot U_{n-1}^k)}{1 + \theta(U_n^k - U_{n-1}^k)} \qquad B\text{-}7b$$

$$PSN = P_n^k + \theta\cdot(P_n^k - P_{n+1}^k)(USN - CSN) \qquad B\text{-}7c$$

$$PRN = P_n^k - \theta\cdot(P_n^k - P_{n-1}^k)(URN + CRN)$$

where $\theta = \frac{\Delta t}{\Delta x}$. CRN and CSN may assume the average value between C_{n-1}^k, C_n^k, and C_{n+1}^k because they vary very little within a couple meshes.

The sequence of computation may be summarized as follows:

1. At the closed end where X=0, equations B-3, B-4b, B-7a, B-7c, and the appropriate boundary conditions should be used.

2. Away from both boundaries, B-1 through B-7 are to be used.

3. At the open end where X = length of gallery, equations B-2, B-4a, B-7b, B-7d and the boundary conditions P = Po (atmospheric pressure) are to be employed.

APPENDIX C.--SYMBOLS LIST

A = Gallery cross-sectional area, m^2.

c = Local sound speed, m sec^{-1}.

c_o = Ambient sound speed, m sec^{-1}.

CRN = Sound speed at the grid point RN, m sec^{-1}.

CSN = Sound speed at the grid point SN, m sec^{-1}.

Cn^k = $c(n\Delta x, k\Delta t)$, m sec^{-1}.

C_+ = Positive characteristic curve identifier.

C_- = Negative characteristic curve identifier.

E = Expansion ratio; that is, ratio of the density of the unburned to the burned gases at the flame front, 1.

f = Darcy-Weisbach friction factor, 1.

γ = Ratio of specific heat, 1.

h = Gallery height, m.

L = Gallery length, m.

L_w = Width of the cross-sectional area, m.

P = Pressure, psi.

P_o = Ambient pressure, psi.

PRN = P at X = RN, psi.

PSN = P at X = SN, psi.

P_n^k = $P(n\Delta x, k\Delta t)$, psi.

SN, RN = Finite difference grid label.

ρ = Density, kg m^{-3}.

Su = Burning velocity, m sec^{-1}.

t = Time, sec.

T = Temperature, K.

Δt = Time increment, sec.

$\tau_{xz}, \tau_w, \tau_{xy}$ = Shearing stress, kg m^{-1} sec^{-2}.

u = Axial velocity, m sec^{-1}.

μ = Viscosity, kgm^{-1} sec^{-1}.

v, w = Velocity in the y and z direction, respectively.

V_b = Volume of the burned gas, m^3.

U.S. GOVERNMENT PRINTING OFFICE: 1975— 606—493:570

INT.-BU.OF MINES,PGH.,PA. 19982